

Journal homepage: <https://modernpathology.org/>

Research Article

Proximal and Classic Epithelioid Sarcomas are Distinct Molecular Entities Defined by MYC/GATA3 and SOX17/Endothelial Markers, Respectively

Luca Sigalotti^a, Anna Maria Frezza^b, Marta Sbaraglia^c, Elisa Del Savio^a, Davide Baldazzi^a, Beatrice Valenti^a, Elena Bellan^d, Ilaria De Benedictis^a, Michele Doni^a, Marco Gambarotti^e, Bruno Vincenzi^f, Antonella Brunello^g, Giacomo Giulio Baldi^h, Emanuela Palmeriniⁱ, Sandro Pasquali^j, Maria Elena Ciuffetti^a, Veronica Varano^a, Filippo Cappello^d, Viviana Appolloni^k, Chiara Pastrello^l, Igor Jurisica^{l,m,n,o}, Alessandro Gronchi^p, Silvia Stacchiotti^b, Paolo Giovanni Casali^{b,q}, Angelo Paolo Dei Tos^c, Roberta Maestro^{a,*}

^a Unit of Oncogenetics and Functional Oncogenomics, Centro di Riferimento Oncologico di Aviano (CRO Aviano) IRCCS, National Cancer Institute, Aviano, Italy; ^b Department of Medical Oncology, Fondazione IRCCS Istituto Nazionale dei Tumori, Milan, Italy; ^c Surgical Pathology and Cytopathology Unit, Department of Medicine-DIMED, University of Padua School of Medicine, Padua, Italy; ^d Department of Pathology, Azienda Ospedale Università Padova, Padua, Italy; ^e Department of Pathology, IRCCS, Istituto Ortopedico Rizzoli, Bologna, Italy; ^f Department of Medical Oncology, Università Campus Biomedico di Roma, Rome, Italy; ^g Department of Oncology, Medical Oncology 1 Unit, Istituto Oncologico Veneto IOV, IRCCS, Padua, Italy; ^h Department of Medical Oncology, Hospital of Prato, Azienda USL Toscana Centro, Prato, Italy; ⁱ Osteoncology, Bone and Soft Tissue Sarcomas and Innovative Therapies, IRCCS, Istituto Ortopedico Rizzoli, Bologna, Italy; ^j Department of Applied Research and Technological Development, Molecular Pharmacology Unit, Fondazione IRCCS Istituto Nazionale dei Tumori, Milan, Italy; ^k Italian Sarcoma Group, Fondazione IRCCS Istituto Nazionale dei Tumori, Milan, Italy; ^l Division of Orthopaedic Surgery, Schroeder Arthritis Institute, Toronto, Canada; ^m Data Science Discovery Centre for Chronic Diseases, Krembil Research Institute, Toronto, Canada; ⁿ Departments of Medical Biophysics and Computer Science, University of Toronto, Toronto, Canada; ^o Institute of Neuroimmunology, Slovak Academy of Sciences, Bratislava, Slovakia; ^p Department of Sarcoma Surgery, Fondazione IRCCS Istituto Nazionale dei Tumori, Milan, Italy; ^q Department of Oncology and Haemato-Oncology, University of Milan, Milan, Italy

ARTICLE INFO

Article history:

Received 14 August 2024

Revised 25 September 2024

Accepted 25 October 2024

Available online 2 November 2024

Keywords:

diagnostic biomarkers
epigenomics
epithelioid sarcoma
next-generation sequencing
soft-tissue sarcoma
transcriptional profiling

ABSTRACT

Epithelioid sarcoma (ES) is a rare tumor hallmark by the loss of INI1/SMARCB1 expression. Apart from this alteration, little is known about the biology of ES. Despite recent advances in treatment, the prognosis of ES remains unsatisfactory. To elucidate the molecular underpinnings of ES, and to identify diagnostic biomarkers and potential therapeutic vulnerabilities, we performed an integrated omics profiling (RNA sequencing and methylation array) of 24 primary, untreated ESs. Transcriptome and methylome analysis identified 2 distinct molecular clusters that essentially corresponded to the morphologic variants of ES, classic ES (C-ES) and the more aggressive proximal ES (P-ES). The P-ES group was characterized by hyperactivation of GATA3 and MYC pathways, with extensive epigenetic rewiring associated with EZH2 overexpression. Both DNA methylation and gene expression analysis indicated a striking similarity with the "MYC subgroup" of atypical teratoid/rhabdoid tumor, another SMARCB1-deficient tumor, implying a shared molecular background and potential therapeutic vulnerabilities. Conversely, the C-ES group exhibited an endothelial-like molecular profile, with expression of vascular genes and elevated proangiogenic SOX17 signaling. Immunohistochemistry validated the overexpression of the chromatin regulators GATA3 (9/12 vs 0/16) and EZH2 (7/7 vs 2/6) in P-ESs, and of the vascular factors SOX17 (8/8 vs 1/10) and N-cadherin (5/

These authors contributed equally: Luca Sigalotti, Anna Maria Frezza, and Marta Sbaraglia.

These authors contributed as colast authors: Angelo Paolo Dei Tos and Roberta Maestro.

* Corresponding author.

E-mail address: rmaestro@cro.it (R. Maestro).



9 vs 0/10) in C-ESs. Therefore, these molecules emerge as potential diagnostic tools to fill the gap represented by the lack of ES subtype-specific biomarkers. In summary, our study shows that P-ES and C-ES represent distinct molecular entities defined by MYC/GATA3 and SOX17/endothelial molecular traits, respectively. Besides providing insights into the biology of ES, our study pinpoints subtype-specific biomarkers and potential therapeutic vulnerabilities.

© 2024 THE AUTHORS. Published by Elsevier Inc. on behalf of the United States & Canadian Academy of Pathology. This is an open access article under the CC BY license (<http://creativecommons.org/licenses/by/4.0/>).

Introduction

Epithelioid sarcoma (ES) is a rare soft tissue sarcoma (incidence 0.02/100,000 in Europe), affecting mostly young and middle-aged patients.^{1,2} The prognosis for ES is poor, with a 5-year overall survival (OS) estimate of ~60% in patients with primary, localized disease, and a median OS of 12 to 18 months in the case of metastatic disease.³⁻⁵ In patients with localized, resectable disease, surgery is the standard of care, sometimes associated with radiation therapy. For patients with unresectable or metastatic disease, treatment options are limited and mostly represented by conventional chemotherapy, pazopanib, and, in the United States, tazemetostat.^{4,5}

Genetically, ES belongs to the class of SMARCB1-loss–driven tumors, which also includes the atypical teratoid/rhabdoid tumor (ATRT) and the malignant rhabdoid tumor (MRT).⁶ These neoplasms are hallmark by the loss of expression of the INI1/SMARCB1 protein, a subunit of the ATP-dependent SWI/SNF chromatin remodeling complexes that support active transcription by fostering chromatin opening. Their activity is opposed by PRC2 chromatin-modifying complexes, which repress gene transcription through EZH2-mediated methylation of histone H3 at K27.^{7,8} Apart from the loss of INI1/SMARCB1 expression, commonly due to the deletion of the SMARCB1 locus at 22q11, no additional recurrent genetic alteration has been detected in ES.^{5,9-12}

Morphologically, ES is a mesenchymal neoplasm characterized by epithelioid cytomorphology and partial epithelial immunophenotype (eg, panCK and EMA expression).¹³⁻¹⁵ The diagnosis of ES may be further refined by subclassifying the tumor into the 2 main morphologic subtypes, “classic-type ES” (C-ES) and the less common “proximal-type ES” (P-ES).¹⁴ Although the nomenclature refers to the fact that C-ES often occurs in acral sites (especially forearm, wrist, and hand, hence the alternative definition of “distal ES”) and P-ES in proximal sites (predominantly pelvis, genitalia, and perineum), the correspondence between subtype and tumor location is not complete, and the misleading terminology is often a source of ambiguity in pathologic and anatomical classification. In general, C-ES shows a nodular arrangement. The nodules are composed of a mixture of eosinophilic epithelioid and spindle cells with mild to overt nuclear atypia. Central degeneration and/or necrosis may be present, often imparting a pseudogranulomatous appearance, particularly evident in larger and/or deep-seated nodules. C-ES commonly shows perivascular and perineural invasion. Mitotic activity is usually low.^{14,15} P-ES usually presents with a multinodular growth pattern and consists of large epithelioid carcinoma-like cells with marked cytologic atypia, vesicular nuclei, and prominent nucleoli. P-ES cells tend to be mitotically active. Tumor necrosis is common but is not associated with the granuloma-like pattern observed in C-ES. P-ES cells often show rhabdoid features with eosinophilic cytoplasm and eccentric vesicular nuclei with large nucleoli. When the rhabdoid phenotype is predominant, the differential diagnosis

with MRT is challenging. Cases showing hybrid histologic features of both C-ES and P-ES have been reported.^{14,15} Although subtype specification may have prognostic relevance, as P-ES is considered a more aggressive tumor,^{2,16,17} it is often omitted from pathology reports because morphologic differences are not always clear-cut, and subtype-specific immunohistochemical markers are lacking.

In an attempt to gain deeper insights into ES biology and identify diagnostic biomarkers and potential therapeutic vulnerabilities, we performed a comprehensive transcriptome and epigenome profiling of a cohort of primary, treatment-naïve ESs. This study was conducted within the framework of the observational, retrospective-prospective EPISObs study on the natural history of ES sponsored by the Italian Sarcoma Group.

Materials and Methods

Patients

This study was conducted on biological samples from patients enrolled in the Italian Sarcoma Group EPISObs study from June 2018 to March 2023. EPISObs is a retrospective-prospective observational study on the natural history of ES ([ClinicalTrials.gov](https://clinicaltrials.gov) NCT03099681).

Histopathology and Immunohistochemistry

A central pathology review was performed for all cases by 2 sarcoma pathology experts (A.P.D.T. and M.S.). Immunohistochemical stainings were performed on 4-μm thick whole sections by using the Bond Polymer Refine Detection Kit (Leica Biosystems) and the BOND-MAX system (Leica Biosystems). Stainings for INI1 (clone MRQ-27, Cell Marque), pan-cytokeratins (clone AE1/AE3, Leica Biosystems), EMA (clone E29, Biocare Medical), and CD34 (clone QBEnd/10, Biocare Medical) were used to support diagnosis. Only ESs showing loss of expression of the INI1/SMARCB1 protein were included in the study. In addition, the expression of GATA3 (clone L50-823, Roche), EZH2 (clone D2C9 XP, Cell Signaling Technology), ERG (clone EP111, Dako), N-cadherin (clone 32/N-Cadherin, BD Biosciences), and SOX17 (polyclonal AF1924, R&D Systems) was evaluated to validate molecular findings. Samples were scored as positive for these markers if >50% of tumor cells stained with an intensity ≥ 3 on a 0 to 5 scale.

RNA Extraction and Whole RNA-Sequencing

RNA extraction and library preparation were essentially as described in Gasparotto et al.¹⁸ In detail, total RNA was extracted from 10-μm formalin-fixed paraffin-embedded (FFPE) tissue sections mounted on glass slides. High tumor cell content (≥60%) areas were marked by the pathologist on a reference hematoxylin–eosin

stained slide and the corresponding areas were scraped on matched unstained slides. The recovered material was dewaxed by means of the Qiagen deparaffinization solution (Qiagen). The RecoverAll Total Nucleic Acid Isolation Kit for FFPE (Thermo Fisher) was used for RNA purification. Whole RNA-sequencing libraries were prepared from 100 to 500 ng total RNA of 24 samples using the Illumina TruSeq Stranded total RNA kit (Illumina) following manufacturer's instructions, and sequenced on an Illumina HiSeq apparatus to an average of 60 million paired-end reads per sample. The quality of the raw sequencing data was evaluated with the FastQC software (RRID:SCR_014583). Reads were aligned to the hg38 reference genome (GRCh38.p13) with STAR v2.7.3.a (RRID:SCR_004463).¹⁹ RSEM v1.3.1 (RRID:SCR_000262)²⁰ was utilized to quantify the reference transcripts, and tximport v1.20.0 was used to summarize transcript data to gene level. The filterByExpr function of edgeR v3.34.1 (RRID:SCR_012802)²¹ was used to filter out low-expressed genes. Analyses here described were conducted on protein-coding gene counts and relative transcript per million (pTPM). Principal component analysis (PCA) and unsupervised hierarchical clustering (Euclidean distance, Ward's linkage) were performed on the top 1000 variant genes, using VST-transformed data generated with DEseq2 v1.32.0 (RRID:SCR_015687).²² The DEseq2 plotPCA function and the ComplexHeatmap v2.8.8 package (RRID:SCR_017270) were used to generate PCA and hierarchical clustering plots, respectively. t-Distributed stochastic neighbor embedding (t-SNE) analysis was performed with the Rtsne v0.15 package on top 1000 variant genes using log2 pTPM+0.1 values, batch-corrected with the removeBatchEffect function of limma v3.50.3 (RRID:SCR_010943). Differential expression analysis was computed with DEseq2. Genes were considered differentially expressed (DE) if |log2 fold change (FC)| ≥ 1 and adjusted P value (*Padj*) $\leq .05$. Boxplots were generated with the ggplot2 v3.3.5 package (RRID:SCR_014601).

Functional Annotation Analysis

Functional annotation of DE genes was performed by overrepresentation analysis using G:Profiler version e107_eg54_p1 7_bf42210 (RRID:SCR_006809).²³ Preranked gene set enrichment analysis (GSEA)²⁴ was carried out with the FGSEA v1.18.0 package (RRID:SCR_020938) using the ranking criteria by Harro et al,²⁵ 10,000 permutations, and FDR ≤ 0.05 . Single-sample GSEA (ssGSEA) was performed with the GSVA v1.40.1 package, and ssGSEA scores were rescaled to a 0 to 10 range. Immune infiltration was evaluated with MCP counter v1.2.²⁶ The immune infiltration score represents the geometric mean of the scores obtained for the immune cell populations. Gene sets used in this work included: Gene ontology-biological processes (GO-BP); Hallmarks gene sets (MSigDB v7.1); a mesenchymal cell signature from Tan and co-workers²⁷; a large artery endothelial cell signature from the endothelial cell atlas (https://endotheliomics.shinyapps.io/ec_atlas)²⁸; genes positively regulated by SOX17 from GSE214742²⁹; a 52-gene signature of EZH2 transcriptional repressive activity obtained by intersecting the genes upregulated by tazemetostat in VA-ES-BJ ES cells (our own data) and in G401 MRT cells³⁰; cell type-specific single-cell RNA-sequencing signatures obtained from The Human Protein Atlas (accessed on October 19, 2023) under the category "cell-type enriched gene sets" (Supplementary Table S1).

Methylation Profiling

Genomic DNA was extracted from FFPE tissue sections by using the AllPrep DNA/RNA kit (Qiagen), and quality was checked with the Infinium HD FFPE QC kit (Illumina). DNA (100 or 250 ng) was

bisulfite converted with the EZ-96 DNA Methylation Kit (Zymo Research), restored with the Infinium HD FFPE DNA Restore Kit (Illumina), and hybridized on Infinium MethylationEPIC v2.0 BeadChips (Illumina). A NextSeq550 instrument (Illumina) was used for array scanning. The resulting raw signal intensities (IDAT files) were preprocessed with the MINFI v1.40.0 package (RRID:SCR_012830),³¹ using published manifest and annotations (https://github.com/jokergoo/IlluminaHumanMethylationEPICv2_manifest; <https://github.com/jokergoo/IlluminaHumanMethylationEPICv2anno.20a1.hg38>) and normalized with the noob option. Probes with detection P value $\geq .01$, overlapping SNP, mapping to sex chromosomes, inaccurately mapped, or cross-hybridizing were removed. t-SNE analysis was performed on beta values of the 10,000 most variable methylation probes using the Rtsne v 0.15 package. t-SNE including different data sets was performed on common probes, normalized, and batch-corrected as described previously.³² Differentially methylated probes (average beta difference $\geq |20\%|$; *q* value $\leq .05$) were identified on M-values by the dmpFinder function from the MINFI package.³¹ Differentially methylated regions (DMR) (mean beta difference $\geq |20\%|$; *P*_{Fisher} $\leq .05$) were identified with the DMRcate package v2.14.0³³ customized for the EPICv2.0 arrays. Annotation of DMR to gene putative regulatory regions (1500 bases upstream and downstream of the transcription start site) was performed with the Annotatr v1.20.0 package. Given the positive effect of promoter demethylation on gene expression, Spearman correlations were performed between expression level [log2(pTPM+0.1)] of DE genes and the mean demethylation value (1- β) of the corresponding regulatory region. Genes mapping to sex chromosomes were excluded from this analysis. Correlations with rho ≥ 0.5 and *P* $\leq .005$ were considered significant. The DKFZ sarcoma and brain tumor classifiers (<https://www.molecularneuropathology.org/mmp>, accessed May 2024)^{32,34} were used to classify ES samples according to methylation profile.

Additional Data Sets

The additional data sets analyzed in this work included: the GSE163359 angiosarcoma RNA-sequencing data set (Gene Expression Omnibus; RRID:SCR_005012)³⁵; the Cancer Genome Atlas (TCGA) sarcoma RNA-sequencing and DNA methylation data sets (<https://www.cancer.gov/tcga>)³⁶ including dedifferentiated liposarcoma (DDLPS), malignant peripheral nerve sheath tumor (MPNST), synovial sarcoma (SS), soft-tissue leiomyosarcoma (STLMS), undifferentiated pleomorphic sarcoma (UPS); the methylation data sets of ATRT (GSE70460), and ES and MRT (GSE140686) generated by the DKFZ group.^{32,37}

Cell Culture and In Vitro Assays

The VA-ES-BJ ES cell line was purchased from the American Type Culture Collection (Manassas). Cells were periodically authenticated by short tandem repeat profiling and evaluated for mycoplasma contamination. Cells were cultured in high glucose Dulbecco's Modified Eagle's Medium (Thermo Fisher Scientific) supplemented with 10% fetal bovine serum (Thermo Fisher Scientific) and maintained at 37°C with 5% CO₂. For drug treatments, cells were seeded in 6-well plates at 75,000 cells per well. After 24 hours, cells were treated with the drug according to the following schedule: 1 μM tazemetostat (Selleckchem) for 15 days (with drug-supplemented medium replenishment every 3 days);

Table 1

Patients characteristics and analyses conducted

ES subtype	Primary site	Sex	Age	Transcriptome	Methylome	Immunohistochemistry
P-ES	Groin	Female	49	✓	✓	✓
	Perineum	Female	47	✓	✓	✓
	Groin	Female	36	✓	✓	✓
	Vulva	Female	35	✓	✓	✓
	Perineum	Female	45	✓	✓	✓
	Trunk	Female	45	✓	✓	✓
	Buttock	Female	70	✓	✓	✓
	Vulva	Female	38	✓	✓	✓
	Groin	Female	32	✓		✓
	Groin	Male	61	✓		✓
	Scrotum	Male	60			✓
	Perineum	Male	26			✓
	Retroperitoneum	Female	49			✓
	Groin	Female	68			✓
C-ES	Hand	Male	16	✓	✓	✓
	Trunk	Male	33	✓	✓	✓
	Leg	Female	20	✓	✓	✓
	Hand	Male	36	✓	✓	✓
	Foot	Male	19	✓	✓	✓
	Forearm	Male	55	✓	✓	✓
	Leg	Female	32	✓	✓	✓
	Buttock	Male	21	✓	✓	✓
	Arm	Male	26	✓		✓
	Forearm	Female	14	✓		✓
	Wrist	Male	28	✓		✓
	Axilla	Male	28	✓		
	Hand	Female	21	✓		
	Forearm	Male	56	✓		
	Hand	Male	25			✓
	Vulva	Female	54			✓
	Forearm	Male	28			✓
	Hand	Male	20			✓
	Hand	Male	8			✓
	Groin	Male	36			✓
	Trunk	Male	34			✓
	Foot	Male	25			✓

ES, epithelioid sarcoma; C-ES, classic ES; P-ES, proximal ES.

1 μM 5-aza-2'-deoxycytidine (DAC) (Selleckchem) for 3 days (with daily drug replenishment) plus 2 days off-drug. An equal volume of the solvent (dimethyl sulfoxide) was used as a control. Total RNA was extracted with miRNeasy Mini Kit (Qiagen) and profiled by RNA-sequencing as described.

Statistical Analysis

Statistical analyses were performed with R v4.1.0.³⁸

Results

Study Cohort

The study was conducted on a subset of primary, treatment-naïve ESs enrolled in the EPISObs trial and for which biological material suitable for immunohistochemical and/or molecular studies was available (Table 1). A central pathology review was performed by 2 sarcoma pathology experts (A.P.D.T. and M.S.). Diagnosis confirmation and classification into P-ES and C-ES were based on morphology, according to the WHO 2020 guidelines.¹⁴ All tumors were characterized by the loss of INI1/SMARCB1

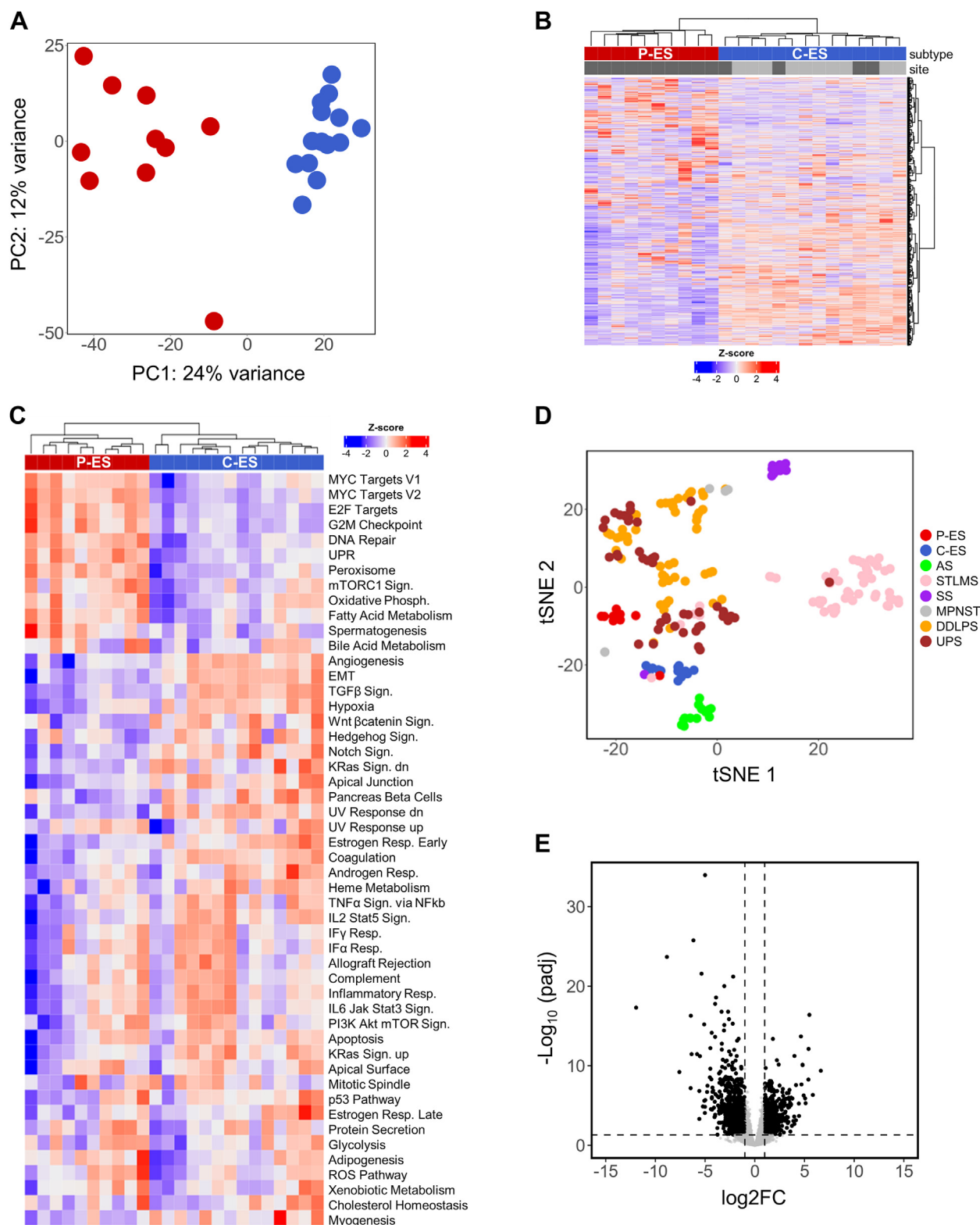
immunoexpression. The median age at presentation was 33.5 years (range, 8–70 years), 46 years for P-ESs (range, 26–70 years), and 27 years for C-ESs (range, 8–56 years). Tumor location was proximal in 21 cases (14/14 P-ESs; 7/22 C-ESs) and distal in 15, all C-ESs (15/22).

Twenty-four cases were selected for molecular analyses based on the suitability of the specimen for omics profiling and a tumor cell fraction ≥ 60%. These included 10 P-ESs (all with proximal location) and 14 C-ESs (10 with distal and 4 with proximal location).

Proximal Epithelioid Sarcoma and Classic Epithelioid Sarcoma Exhibit Profoundly Different Transcriptional Profiles

To identify molecularly distinct ES groups in an unbiased manner, transcriptome data were analyzed by unsupervised hierarchical clustering, PCA, and activation of molecular signatures, as assessed by ssGSEA. All these approaches identified 2 separate clusters, which essentially corresponded to the morphologic subtypes, P-ES and C-ES (Fig. 1A–C).

Intriguingly, one sample, originally classified as P-ES, was found to cluster with C-ESs. The histologic revision resulted in a reclassification of this case as a C-ES with a confusing high-grade

**Figure 1.**

Unsupervised analysis of ES transcriptome. (A) PCA calculated on the top 1000 variant genes. C-ESs are labeled in blue; P-ESs in red. (B) Unsupervised hierarchical clustering. The heatmap reports Z-score normalized expression values of the top 1000 variant genes. Anatomical site: dark gray, proximal site; light gray, distal site. (C) Unsupervised hierarchical clustering of ssGSEA scores for MSigDB hallmarks. (D) t-SNE calculated on top 1000 variant genes. AS, angiosarcoma; DDLPS, dedifferentiated liposarcoma; MPNST, malignant peripheral nerve sheath tumor; SS, synovial sarcoma; STLMS, soft tissue leiomyosarcoma; UPS, undifferentiated pleiomorphic sarcoma. (E) Volcano plot of differentially expressed genes in P-ES vs C-ES. Black dots identify differentially expressed genes ($|\log_2\text{FC}| \geq 1$; $\text{Padj} \leq .05$). Genes overexpressed in P-ESs (X-axis positive values) are on the right, C-ES overexpressed genes are on the left. ES, epithelioid sarcoma; C-ES, classic epithelioid sarcoma; PCA, principal component analysis; P-ES, proximal epithelioid sarcoma; ssGSEA, single-sample gene set enrichment analysis; t-SNE, t-distributed stochastic neighbor embedding.

morphology, supporting the notion that the diagnosis of P-ES and C-ES often relies on subtle morphologic differences and may fail to catch their molecular diversities. Tumor location had no impact on the transcriptome, as all C-ESs clustered together, regardless of their distal or proximal anatomical location (Fig. 1B). These results indicate that P-ES and C-ES histologic subtypes do exhibit a distinct transcriptional profile and biological pathway activations. To gauge the extent of diversity in the transcriptional profile of the 2 ES subtypes, RNA-seq data from ESs were combined with data from an independent cohort of sarcomas of different histologies (TCGA sarcoma plus angiosarcoma data sets). t-SNE analysis showed that even in this more complex scenario, C-ESs and P-ESs continued to form separate clusters (Fig. 1D), corroborating the profound molecular differences between the 2 subtypes.

Proximal Epithelioid Sarcoma is Characterized by a MYC Transcriptional Profile and Overexpression of Chromatin Rewiring Genes

Differential expression analysis indicated that 753 genes were upregulated and 1017 downregulated in the P-ES vs C-ES comparison (Fig. 1E; Supplementary Table S2A). GSEA and overrepresentation analysis of DE genes showed enrichment in P-ES of processes involved in cell proliferation, protein metabolism, including mTORC1 signaling and unfolded protein response, and chromatin rewiring (Fig. 2A, B; Supplementary Table S2B-D). The enrichment of cell proliferation molecules in P-ESs was associated with a higher mitotic count (mean mitosis score, 2.3 in P-ESs vs 1.4 in C-ESs) and was paralleled by overexpression of proproliferative transcription factors such as *MYC* and *E2F*, and corresponding targets. Intriguingly, the *CDK4/CDK6* ratio was inverted in P-ESs and C-ESs (Fig. 2B, C, Supplementary Table S2A). Genes involved in ribosome biogenesis and elongation factors were also overexpressed in P-ESs, in line with the implication of *MYC:mTORC1* interplay in regulating protein synthesis³⁹ (Fig. 2B, Supplementary Table S2A). Noteworthy, *MYC*, mTORC1, and unfolded protein response signalings were higher in P-ESs not only compared with C-ESs but also compared with other sarcoma histotypes (Fig. 2D).

Several epigenetic regulators were upregulated in P-ESs. These included subunits of chromatin remodeling complexes (*HELLS* and *CDC47*), chromatin architectural proteins (*HMG2A*), and components of the PRC1/PRC2 chromatin-modifying complexes such as *CBX6*, *EZH2*, and *EZH2*-associated molecules (*AEBP2* and *ZMYND8*). Moreover, in keeping with its ability to induce *MYC* expression,⁴⁰ the chromatin opener and pioneer transcription factor *GATA3* was selectively expressed in P-ESs (Fig. 2C and Supplementary Table S2A).

The relevance of chromatin rewiring in P-ES biology was corroborated by the finding that an *EZH2* activity score (calculated by ssGSEA on the signature derived by intersecting the list of genes induced by tazemetostat in 2 SMARCB1-deficient sarcoma cell lines), was particularly increased in this ES subtype as it was in synovial sarcoma, a prototype of PRC2 functionally altered tumor (Fig. 2D).

Classic Epithelioid Sarcoma Transcriptome Indicates a Link with the Endothelial Lineage and SOX17 Pathway

Genes upregulated in C-ESs were involved in biological processes related to vasculature, mesoderm development, and extracellular matrix organization (Fig. 3A, B). C-ESs featured

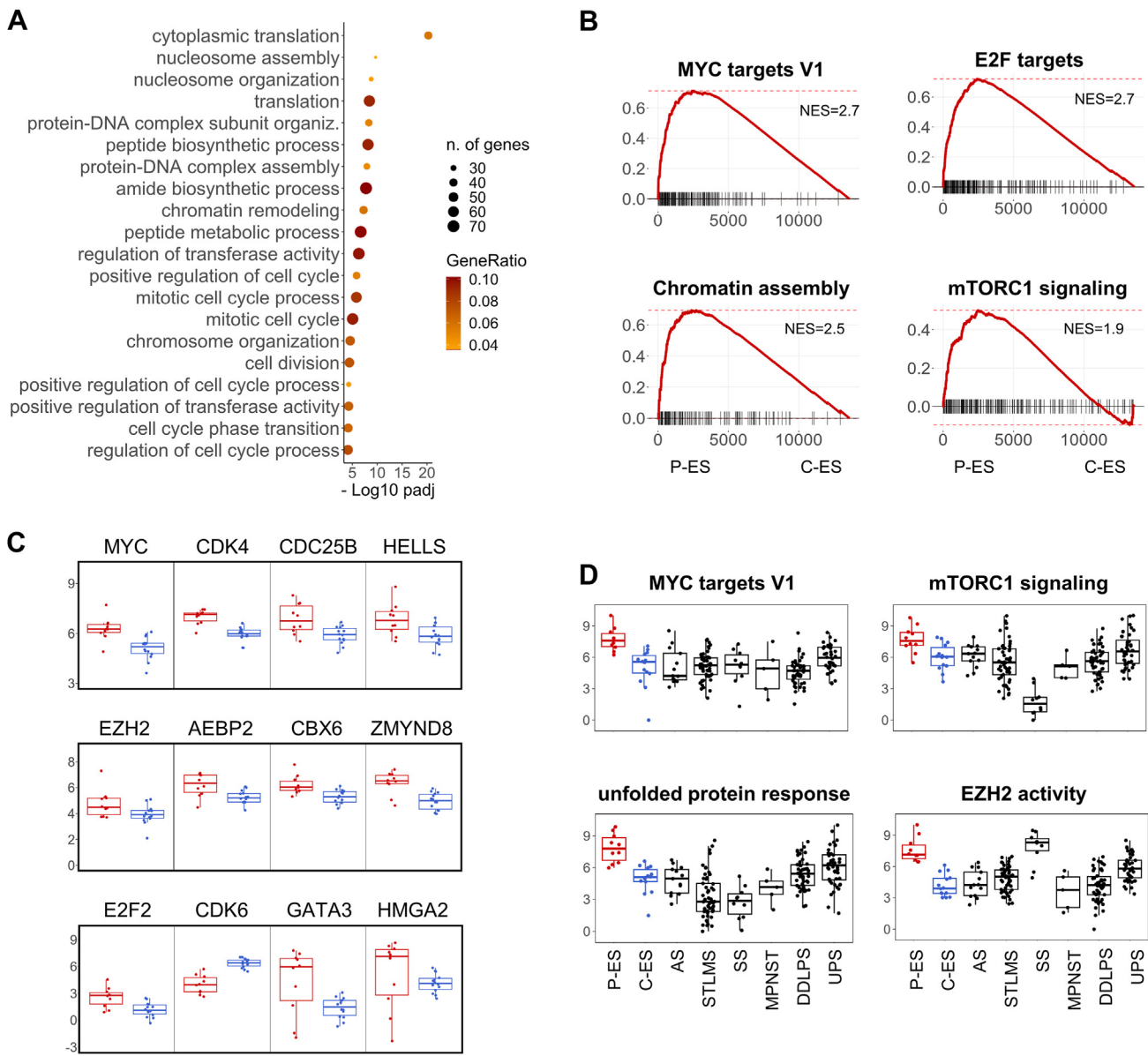
overexpression of several collagens, matrix metalloproteases, and genes related to the epithelial-mesenchymal transition, in line with a previous report.⁹ Intriguingly, although no difference in vascularization was observed between the 2 ES subtypes, the C-ES transcriptome showed elevated levels of genes involved in the development of the endothelium. Upregulated vascular genes included the tyrosine kinase *TEK* and its ligand *ANGPT1*, endothelin (*EDN1*), VE-cadherin (*CDH5*), and N-cadherin (*CDH2*), which are the 2 main cadherins expressed by endothelial cells, and *CD109*. Endothelial-related transcription factors overexpressed in C-ESs included *ERG*, *ETS1*, *FLI1*, *TAL1*, *RUNX1*, and *SOX17*, the latter being particularly upregulated (Fig. 3C; Supplementary Fig. S1; Supplementary Table S2A-D). To better appreciate the biological relevance of this finding, we compared the expression of these vascular-related genes in ESs vs other sarcoma histotypes (TCGA sarcoma and angiosarcoma data sets): most of these molecules were expressed in C-ESs at levels that were similar to those detected in vasculogenic tumors (angiosarcomas) and higher than those found in non-vasculogenic sarcomas (Fig. 3C). Accordingly, similar to angiosarcomas, C-ESs showed enrichment for angiogenic signatures, including a *SOX17*-specific and an endothelial cell-specific signature (Fig. 3D-E), supporting a relationship of C-ES with the endothelial lineage.

As an aside, similar to what was reported in a recent study,⁹ DE analysis showed an apparent upregulation of *SMARCB1* in C-ESs, although not as a top-ranked DE gene. This was a puzzling result because not only both ES subtypes are characterized by *INI1/SMARCB1* protein loss, but several C-ESs included in our study were homozygously deleted for *SMARCB1*. Although all samples were selected for having a high tumor cell content ($\geq 60\%$), a closer examination of ES specimens revealed a relatively higher presence of nontumor (*SMARCB1*-positive) cells in C-ESs, in line with the infiltrative growth pattern and immune infiltrate commonly observed in this ES subtype.⁴¹ Accordingly, *SMARCB1* mRNA levels correlated inversely with the tumor cell fraction and directly with the estimated immune infiltrate (Supplementary Fig. S2A, B). These findings underscore the importance of a careful morphologic evaluation of tumor specimens when conducting bulk omics analyses.

Proximal Epithelioid Sarcoma and Classic Epithelioid Sarcoma Display Distinct DNA Methylation Profiles

In keeping with previous reports,⁹ DNA mutation and copy number variation analysis failed to reveal recurrent genetic alterations describing the 2 ES subtypes (data not shown). Instead, significant differences emerged from genome-wide DNA methylation profiling of 8 P-ESs and 8 C-ESs: unsupervised analysis of ES methylome demonstrated a clear separation between the 2 subtypes (Fig. 4A, B), indicating a role for epigenetics in determining the molecular differences between P-ES and C-ES. To assess the robustness of this separation and identify groups of tumors with similar methylation patterns, the methylation data from our ES samples and the TCGA sarcoma data set were pooled and interrogated as a whole by t-SNE. Even in this more complex scenario, C-ESs and P-ESs clustered apart (Fig. 4C), further supporting the notion that they are epigenetically different and represent discrete biological entities.

Approximately 15% of the probes were differentially methylated in P-ES vs C-ES, with a marked skew toward hypermethylation in P-ESs (ie, hypomethylation in C-ESs) (Supplementary Fig. S3A). Since the regulatory regions of

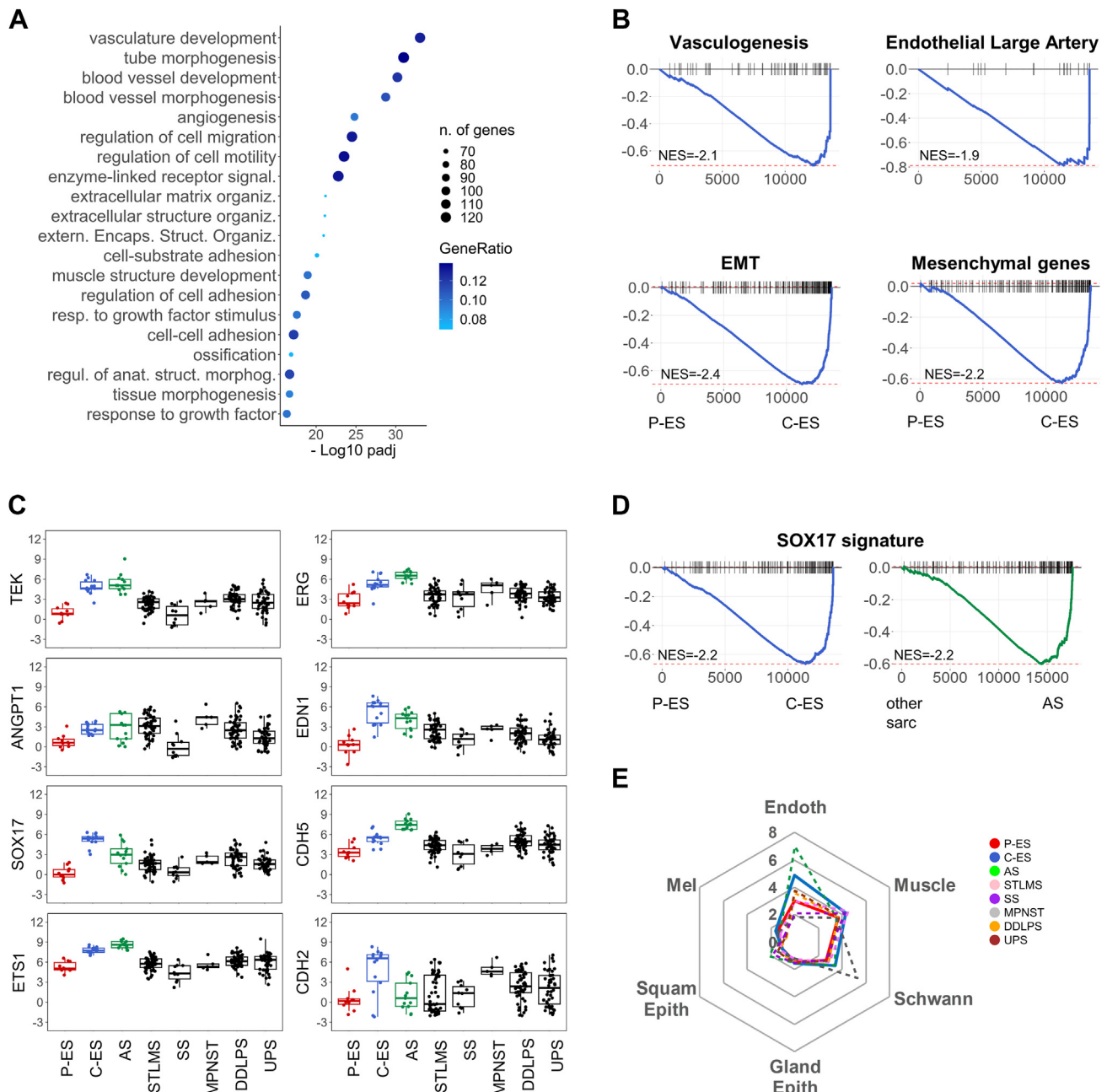
**Figure 2.**

Functional annotation of P-ES transcriptome. (A) Overrepresentation analysis of GO biological processes enriched in P-ES. The analysis was run on genes upregulated in P-ES vs C-ES ($\text{Padj} \leq .05$, $\log 2\text{FC} \geq 1$). Top 20 terms by Padj are shown. (B) Representative prereduced GSEA plots against the indicated gene sets. The enrichment score is on the y-axis. The x-axis reports the ranked gene list, from P-ES (left) to C-ES (right). NES, normalized enrichment score. (C) Boxplots representative of cell cycle and chromatin metabolism genes upregulated in P-ES (red) vs C-ES (blue) ($\text{Padj} \leq .05$, $\log 2\text{FC} \geq 1$). The Y-axis reports the expression values in $\log 2(\text{TPM} + 0.1)$. The box indicates the IQR and the line within the median value. (D) MYC, mTORC1, UPR, and EZH2 activity scores evaluated by ssGSEA in P-ESs, C-ESs, and other sarcomas. C-ES, classic epithelioid sarcoma; P-ES, proximal epithelioid sarcoma; ssGSEA, single-sample gene set enrichment analysis.

transcriptionally active genes are usually hypomethylated, we performed a functional annotation of the genes showing this characteristic. This approach indicated that hypomethylated genes in C-ESs were largely involved in vascular development, suggesting that relief of DNA methylation may account for the activation of this pathway in this ES subtype (Fig. 4D). Indeed, a statistically significant correlation between demethylation of the regulatory region and expression level was detected in about 24% (235/972) of the genes upregulated in C-ESs and only 8% (58/710) of the genes upregulated in P-ESs. Genes hypomethylated in C-ESs whose expression correlated with demethylation extent included *ETS1*, *TEK*, and its ligand angiopoietin 1 (*ANGPT1*) (Fig. 4E). The role of DNA methylation in the regulation of these genes was

confirmed by transcriptional profiling of an ES cell line treated with the demethylating agent DAC (Supplementary Fig. S3B). Taken together, these results indicate that epigenetics plays an important role in shaping the transcriptome of the 2 ES subtypes.

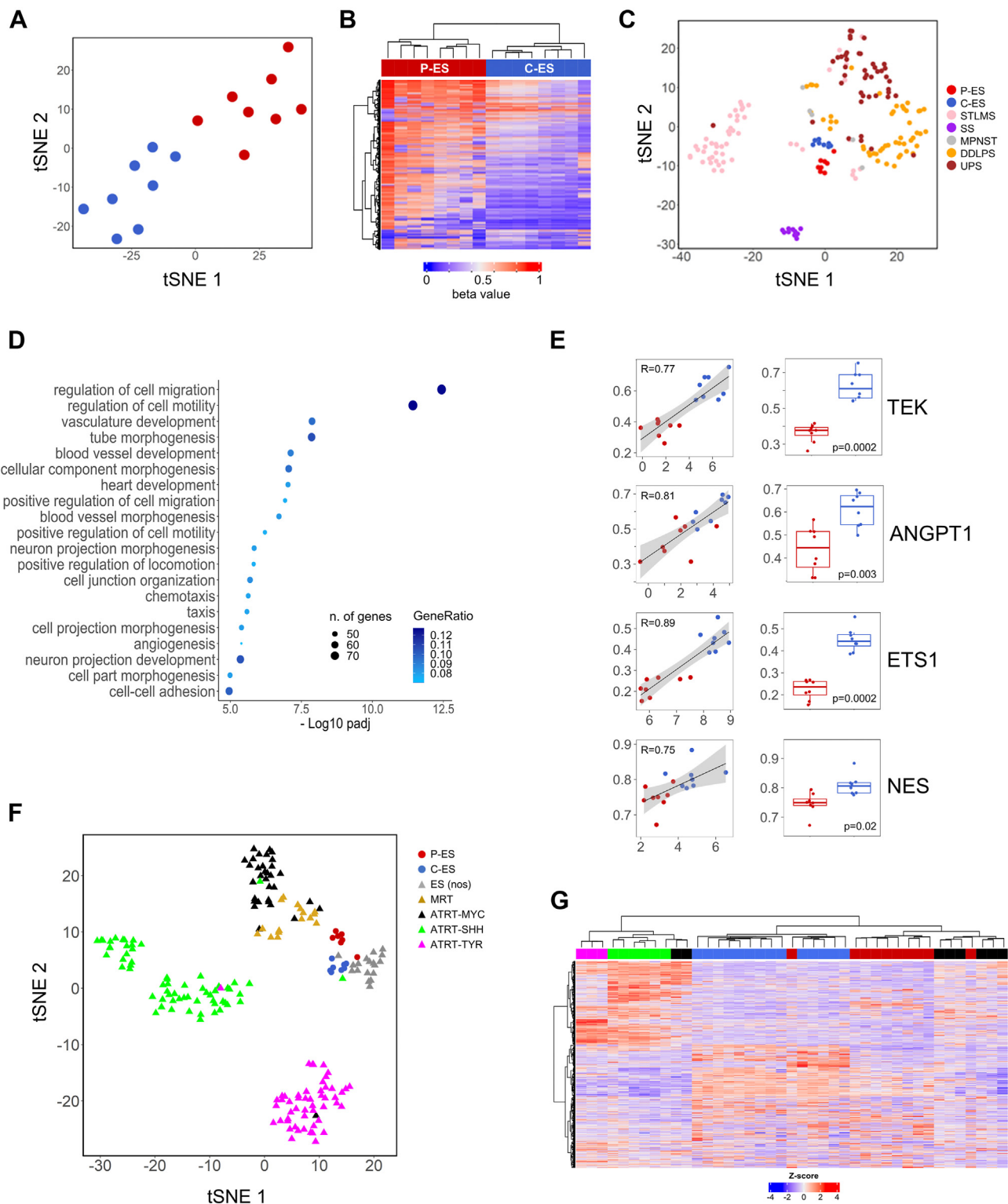
Finally, we sought to evaluate the performance of the sarcoma classification system developed by the DKFZ group that predicts tumor histology based on DNA methylation patterns.³² Given the common genetics with ATRT (SMARCB1 deficiency), the DKFZ brain tumor classifier was also utilized. Only 5/16 ESs were actually scored as ES by the DKFZ sarcoma classifier, 3 with high confidence (score ≥ 0.9) and 2 with medium confidence (0.5 < score < 0.9). Of the 8 P-ESs included in the series, 3 were classified as MRT by the sarcoma classifier (1 with high and 2 with medium confidence), in

**Figure 3.**

Functional annotation of C-ES transcriptome. (A) Overrepresentation analysis of GO biological processes enriched in C-ESs. The analysis was run on genes upregulated in C-ESs vs P-ESs. (B) Representative preranked GSEA plots against the indicated gene sets. (C) Boxplots representative of vascular-related molecules in P-ES (red), C-ES (blue), AS (green), and other sarcomas (black). The Y-axis reports the expression values in $\log_2(p\text{TPM}+0.1)$. (D) Preranked GSEA enrichment plots against a SOX17 signature (SOX17 positively regulated genes) for P-ES vs C-ES (left) and TCGA sarcoma types vs AS (right). (E) The same tumor series as in C was analyzed by ssGSEA against cell-type-specific signatures (single-cell RNA-sequencing data) obtained from The Human Protein Atlas. The scores reported represent the geometric mean of each cell-specific score. Endothelial cells (Endoth), muscle cells (Muscle), Schwann cells (Schwann), glandular epithelial cells (Gland Epith), squamous epithelial cells (Squam Epith), melanocytes (Mel). ATRT, atypical teratoid/rhabdoid tumor; C-ES, classic epithelioid sarcoma; GSEA, gene set enrichment analysis; P-ES, proximal epithelioid sarcoma; ssGSEA, single-sample gene set enrichment analysis.

line with the reported morphologic and immunophenotypic overlap with this tumor,^{14,15} and 4 P-ESs were classified as ATRT-MYC by the DKFZ brain classifier (2 with high and 2 with medium confidence) (Supplementary Table S3). In light of this result, we performed a clustering analysis on the methylation data of our ES series combined with the data generated by the DKFZ group on MRT, ATRT, and ES (not distinguished into subtypes). t-SNE showed that P-ESs formed a group that

mapped in proximity to the cluster composed of ATRT-MYC and MRT samples, both tumor types characterized by MYC activation,⁴² supporting a molecular similarity of P-ES with these entities (Fig. 4F). Analysis of RNA-sequencing data further corroborated this concept, as P-ES and ATRT-MYC transcriptomes coclustered in unsupervised hierarchical clustering and shared MYC, EZH2, and mTORC1 pathway activation (Fig. 4G and Supplementary Fig. S4A, B).

**Figure 4.**

DNA methylation profiling of ES. t-SNE (A) and unsupervised hierarchical clustering (B) on the top 10,000 variant methylation probes in C-ESs (blue) and P-ESs (red). (C) t-SNE of ES and the TCGA sarcoma series. (D) Overrepresentation analysis on GO-BP of the genes mapping to the regions hypomethylated in C-ESs. (E) Left panels: a representative set of genes showing a significant correlation ($\rho \geq 0.5$; $P \leq .005$) between the mean demethylation status of the regulatory region ($1-\beta$) on the Y-axis and transcript expression levels ($\log_{2}2\text{pTPM}$) on the X-axis; right panels: box plots of mean demethylation status of the regulatory region ($1-\beta$) in P-ESs (red) and C-ESs (blue). Shading indicates the CI. (F) t-SNE of our series of P-ESs and C-ESs, in relation to the methylation data of other tumors, including ES (not otherwise specified, ES nos) (GSE70460), MRT (GSE70460), and ATRT (GSE140686) of the DKFZ group. (G) Hierarchical clustering of the transcriptome of P-ESs and C-ESs together with ATRT transcriptome data from GSE243682 and GSE242090 (color code as in F). ATRT, atypical teratoid/rhabdoid tumor; C-ES, classic epithelioid sarcoma; ES, epithelioid sarcoma; GO-BP, gene ontology-biological processes; MRT, malignant rhabdoid tumor; P-ES, proximal epithelioid sarcoma; t-SNE, t-distributed stochastic neighbor embedding

Table 2

Immunohistochemical validation of selected biomarkers

ES subtype	Primary site	GATA3	EZH2	SOX17	N-cadherin (CDH2)	ERG
P-ES	Buttock	+	+	—	—	—
	Perineum	+	+	—	—	—
	Perineum	—	+	—	—	—
	Groin	+	+	—	—	—
	Vulva	+	+	—	—	—
	Vulva	+	+	—	—	—
	Scrotum	+	—	—	—	—
	Groin	—	—	—	—	—
	Trunk	+	—	—	—	—
	Groin	—	—	—	—	—
	Perineum	+	—	—	—	—
	Groin	+	—	—	—	—
	Groin	—	—	—	—	—
	Retropertitoneum	—	—	—	—	—
C-ES	Leg	—	—	—	—	—
	Arm	—	—	—	+	—
	Trunk	—	—	+	+	—
	Forearm	—	—	—	—	—
	Hand	—	—	+	—	—
	Arm	—	—	—	—	—
	Wrist	—	—	—	—	—
	Forearm	—	—	—	—	—
	Hand	—	—	—	—	—
	Hand	—	—	—	—	—
	Groin	—	—	—	+	—
	Foot	—	—	+	—	+
	Forearm	—	—	+	—	+
	Leg	—	+	+	+	—
	Hand	—	—	—	+	—
	Vulva	—	—	+	—	+
	Trunk	—	—	+	—	—
	Foot	—	+	+	—	—
Specificity	100.0 (79.4-100.0)	66.7 (22.3-95.7)	90.0 (55.5-99.8)	100.0 (69.2-100.0)	100 (59.0-100.0)	—
Sensitivity	75.0 (42.8-94.5)	100.0 (59.0-100.0)	100.0 (63.1-100.0)	55.6 (21.2-86.3)	33.3 (7.5-70.1)	—
Accuracy	89.3 (71.8-97.7)	84.6 (54.6-98.1)	94.4 (72.7-99.9)	79.0 (54.4-94.0)	62.5 (35.4-84.8)	—

ES, epithelioid sarcoma; C-ES, classic ES; P-ES, proximal ES.

Samples were scored as positive (+) if >50% tumor cells stained with an intensity ≥ 3 in a 0-5 scale.

Specificity, sensitivity, accuracy, and relative confidence intervals (between brackets), are in %.

Detailed information on the percentage of positive tumor cells and immunostaining intensity is provided in [Supplementary Table S4](#).

Immunohistochemistry Validates Subtype-Specific Biomarkers

Given the different prognosis of the 2 ES subtypes and the possible uncertainty in subtype classification that relies solely on morphology, we investigated the diagnostic utility of the molecules identified as differentially expressed in P-ES vs C-ES. Candidates were selected based on the extent of differential expression and the availability of immunohistochemistry-validated antibodies. On these grounds, *GATA3* and *EZH2* were selected as potential P-ES markers; *SOX17*, N-cadherin/CDH2, and *ERG* were chosen for C-ES. Unfortunately, although *TEK* stood out as a potential strong C-ES marker, none of the tested *TEK* antibodies demonstrated to work on FFPE samples.

In line with transcriptomic data, immunohistochemistry confirmed the selective positivity for *GATA3* in P-ESs ([Table 2](#), [Supplementary Table S4](#), [Fig. 5](#)). A moderate-to-strong *GATA3* nuclear immunoreactivity was detected in 9/12 P-ESs tested (75%); vice versa, all C-ESs analyzed were negative (16/16). *EZH2* was expressed in all ESs tested. However, a diffuse (>50% of tumor nuclei) and moderate-to-strong nuclear immunoreaction for anti-*EZH2* antibodies was observed in 7/7 P-ESs and 2/6 C-ESs.

Some nonspecific weak/weak-to-moderate staining in a few cells was detected with the *SOX17* and N-cadherin/CDH2 antibodies employed. However, diffuse and moderate-to-strong *SOX17* nuclear positivity was detected almost exclusively in C-ESs (8/8 C-ESs; 1/10 P-ESs). The same held true for N-cadherin/CDH2, and *ERG*: 5/9 C-ESs showed a cytoplasmic/membranous N-cadherin staining and 3/9 C-ESs displayed nuclear *ERG* immunoreactivity. All P-ESs were scored negative for these markers. Overall, immunohistochemical analyses validated RNA-seq data and the potential utility of the identified markers in distinguishing the 2 ES subtypes.

Discussion

In this study, we provide evidence that P-ES and C-ES represent 2 distinct molecular entities marked by profoundly different transcriptional and DNA methylation profiles. P-ESs showed enrichment in pathways implicated in protein synthesis, chromatin metabolism, and cell proliferation, with increased MYC signaling. Due to the negative control exerted by SMARCB1 on MYC transcription and activity,^{43,44} MYC pathway activation is a

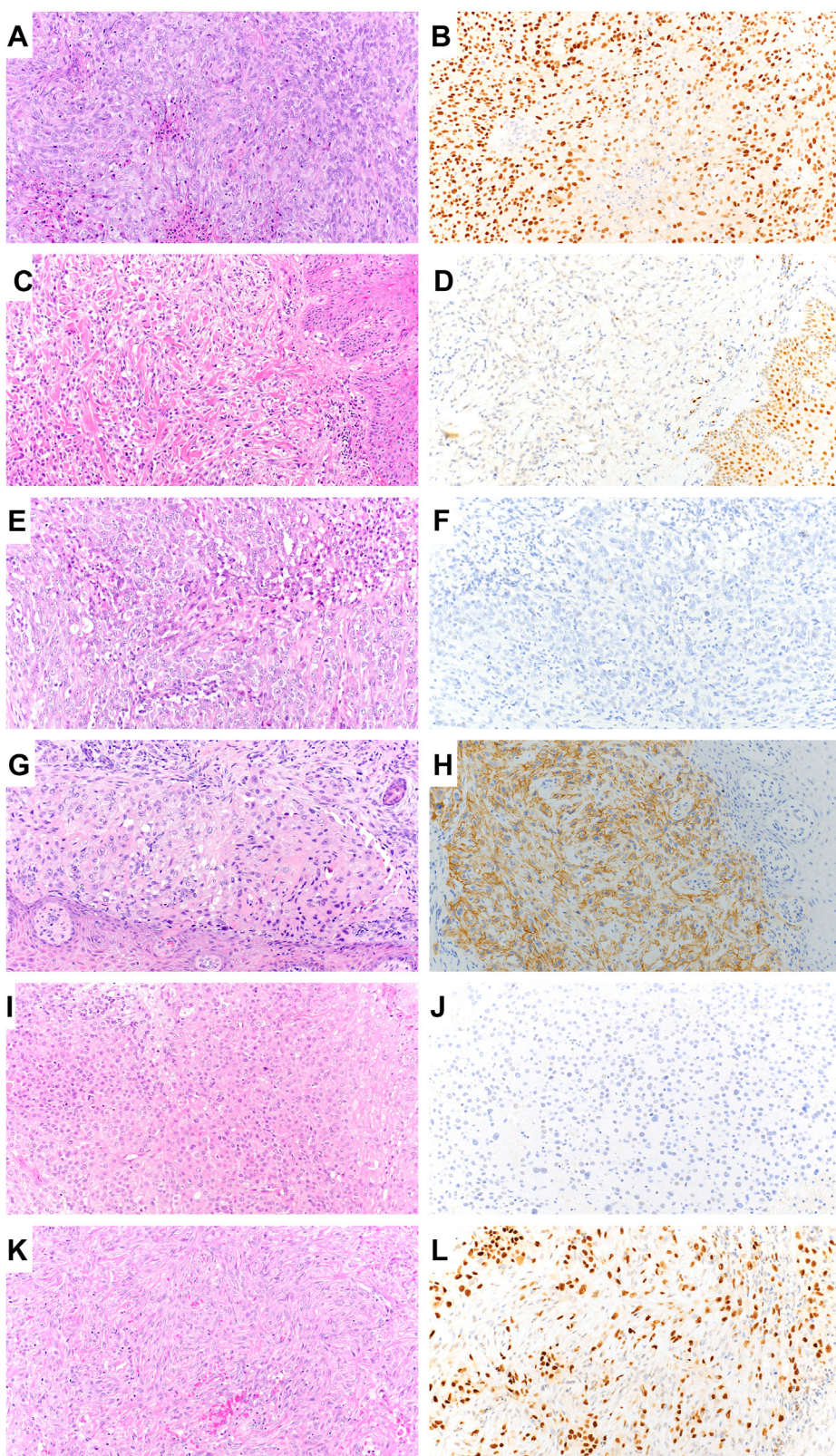


Figure 5.

Representative hematoxylin-eosin images (left panels) and immunostainings (right panels) of P-ES and C-ES. (A, B) P-ES showing strong and diffuse expression of GATA3 in tumor cell nuclei. (C, D) GATA3 negative staining in a CES; GATA3 immunoreactivity was observed in keratinocytes and lymphocytes (right corner). (E, F) Negative staining for N-cadherin/CDH2 in a P-ES. (G, H) C-ES showing cytoplasmic and membranous staining for N-cadherin/CDH2. (I) P-ES negative for SOX17 staining. (K, L) Positive nuclear staining for SOX17 in C-ES tumor cells. P-ES samples are composed of large epithelioid cells showing vesicular nuclei, marked nucleoli, and abundant eosinophilic cytoplasm with occasional rhabdoid morphology. C-ES samples show atypical epithelioid and spindle cells, and an infiltrative pattern of growth. C-ES, classic epithelioid sarcoma; P-ES, proximal epithelioid sarcoma.

common finding in SMARCB1-defective tumors. Yet, a full-blown "MYC phenotype" has been reported for the MYC molecular subgroup of ATRT (ATRT-MYC).³⁷ Intriguingly, RNA-sequencing analysis showed that the transcriptome profile of P-ES was similar to that of ATRT-MYC and that these tumors shared the activation of common pathways including MYC, EZH2, and mTORC1. The biological affinity between P-ES and ATRT-MYC was also supported by the similarity of their DNA methylation profiles and by the finding that the DKFZ methylation classifiers indicated a diagnosis compatible with ATRT-MYC for 4/8 P-ESs. Noteworthy, MYC-driven transactivation is potentiated by GATA3,⁴⁰ which we found to be selectively overexpressed in P-ESs. Therefore, MYC hyperactivation and GATA3 expression are unique hallmarks of P-ES and, in analogy to ATRT-MYC, we propose that P-ES represents the MYC molecular subset of ESs (ES-MYC).

P-ESs also expressed elevated levels of several chromatin metabolism genes, including *EZH2* and *HELLS*, and showed a markedly hypermethylated genome, implicating epigenetic rewiring in P-ES pathobiology. Noteworthy, *EZH2* is induced by MYC,^{45,46} and the expression of *EZH2*, *HELLS*, and *GATA3* has been associated with poor outcomes in several neoplasms.⁴⁷⁻⁵⁰ Thus, the combined effect of chromatin modifiers' overactivation and extensive DNA methylation is likely to play an important role in the diversity of the 2 ES subtypes and, possibly, in the aggressive clinical course of P-ES.

C-ESs featured enrichment in mesenchymal features and extracellular matrix components, in agreement with a previous study.⁹ Particularly intriguing was the link with the endothelium. In fact, the functional annotation of the genes demethylated and overexpressed in C-ESs demonstrated a clear enrichment for pathways associated with vascular development, and several endothelial genes (eg, *SOX17*, *TEK*, *ERG*, *ETS1*, VE-cadherin, and N-cadherin) showed expression levels close to those of an overt vascular tumor such as angiosarcoma. Notably, *SOX17* has been shown to promote the conversion of human fibroblasts into endothelial cells,^{51,52} suggesting a major role for this molecule in the phenotypic drift of C-ES. Importantly, the specific expression by C-ES tumor cells of endothelial markers, namely, *ERG*, N-cadherin, and *SOX17*, was confirmed by immunohistochemistry. Unfortunately, we failed to find FFPE-compatible commercial TEK-specific antibodies to orthogonally validate its remarkable transcriptional upregulation in C-ESs. A possible endothelial differentiation of ES was originally proposed in 1998 by Smith et al,⁵³ based on the positive staining for VE-cadherin and negativity for E-cadherin. Several authors have subsequently reported the expression of *ERG*, *FLI1*, and podoplanin in a fraction of ESs, primarily C-ESs, but the link with endothelial lineage remained debated due to the incomplete expression of vascular markers.⁵⁴⁻⁵⁶ Our integrated omics profiling supports the existence of this connection.

We acknowledge that our molecular study was conducted on a relatively limited number of cases. On one hand, this is justified by the extreme rarity of the disease. On the other hand, the stringent criteria applied for sample inclusion in the omics analyses (patients enrolled in the EPISObs clinical study; treatment-naïve primary tumors; diagnosis confirmed by central pathology review with verified loss of INI1/SMARCB1 protein expression; biospecimens with a tumor cell fraction $\geq 60\%$) contributed to narrow down the number of enrollable samples, but at the same time enabled us to control for confounding factors that could affect the biological interpretation of the data and to better appreciate the distinctive molecular features of P-ES and C-ES tumor cells.

In summary, our study demonstrates that P-ES and C-ES exhibit strikingly divergent transcriptome and DNA methylome

profiles, thereby identifying biologically different entities. P-ES is typified by a MYC/GATA3 phenotype and epigenetic rewiring. In contrast, C-ES shows a link with the endothelial lineage and hyperactivation of *SOX17* signaling. GATA3, N-cadherin, and *SOX17* emerge as potential immunohistochemical markers for subtype-specific diagnosis. From a clinical perspective, our results disclose some attractive scenarios. Currently, for patients with ES with unresectable or metastatic disease, treatment options are unsatisfactory. Conventional chemotherapeutic regimens demonstrate limited efficacy, achieving <27% overall responses with a median response duration of <6 months.⁴ In the United States, the introduction of tazemetostat has only marginally improved ES outcomes, with most patients being resistant to this therapy. Unfortunately, the original work did not report the breakdown of tazemetostat response by ES morphologic subtype.^{5,57} It would be interesting to assess whether a measure of *EZH2* activity may have a predictive value. On the other hand, the substantial similarities found between P-ES and ATRT-MYC suggest that the therapeutic strategies currently being explored for the treatment of this brain tumor could also have potential for P-ES: BET inhibitors have revealed antitumor activity in ATRT-MYC preclinical models^{58,59}; bortezomib has proven to be particularly effective in targeting MYC-hyperactive tumors, including ATRT-MYC; several studies demonstrated that ATRT-MYC cell lines are sensitive to mTORC1 inhibition.^{58,60,61} Conversely, the peculiar overexpression of TEK in C-ESs is appealing as the TEK pathway inhibitors are currently under evaluation in different solid tumors.^{62,63} The development of subtype-specific ES cell models and xenografts will be key to addressing these hypotheses.

Acknowledgments

Results shown in this manuscript are in part based on data generated by TCGA Research Network: <https://www.cancer.gov/tcga>. In particular, the transcriptome analyses of the data set indicated in this publication as the "TCGA sarcoma data set" are based on the authorized use of study data downloaded from dbGaP web site (<https://www.ncbi.nlm.nih.gov/gap/>), under phs000178.v11.p8.c1 (Project authorization #22596 to R.M.).

The authors are grateful to the Italian Sarcoma Group for supporting the clinical coordination of the EPISObs study.

Author Contributions

L.S. performed conceptualization, formal analysis, investigation, and writing the original draft. A.M.F., A.G., and S.S. performed clinical study design, sample collection, and contributed toward the clinical study and review and editing of the draft. M.S. and E.D.S. performed formal analysis, investigation, and writing the original draft. D.B., M.D., C.P., and I.J. contributed to formal analysis. Be.Va., E.B., I.D.B., M.E.C., V.V., and F.C. performed investigation. M.G., B.V., A.B., G.G.B., E.P., S.P., and V.A. made sample collection and contributed to the clinical study. P.G.C. performed clinical study design and review and editing of the draft. A.P.D.T. performed conceptualization, supervision, and writing the original draft. R.M. performed conceptualization, supervision, funding acquisition, and writing the original draft.

Data Availability

All relevant data are included in the manuscript or provided as supplementary material.

Funding

This work was supported by the Italian Ministry of Health-Ricerca Corrente; 5 per mille CRO Aviano funds (Italian Ministry of Health), institutional grant to R.M.; Italian Ministry of Health/Alleanza Contro il Cancro (ACC) to R.M.; Associazione Italiana Ricerca sul Cancro (AIRC #19975) to R.M.; 5 per 1000 funds (2019 Italian Ministry of Health, financial support for health care research) institutional grant BRI 2021 to A.M.F.; Associazione Orchestra Per la Vita-ONLUS.

Declaration of Competing Interests

A.M.F. declares institutional research funding from Advenchen Laboratories, Amgen Dompé, Bayer, Blueprint Medicines, Daiichi Sankyo, Deciphera, Eisai, Eli Lilly, Epizyme Inc, GlaxoSmithKline, Karyopharm Pharmaceuticals, Novartis, Pfizer, and PharmaMar. A.B. declares consulting/advisory role for GlaxoSmithKline, and PharmaMar; support for attending meetings and/or travels from PharmaMar. G.G.B. declares honoraria from PharmaMar, Eli Lilly, GlaxoSmithKline, Merck Sharp & Dome, Eisai, and Istituto Gentili; consulting/advisory role from PharmaMar, Eli Lilly, GlaxoSmithKline, Merck Sharp & Dome, and Eisai; support for attending meetings and/or travels from Novartis, PharmaMar, and Eli Lilly. E.P. declares consulting/advisory roles for Daiichi Sankyo, Deciphera, and SynOX. S.P. declares institutional research funding from Ikena Oncology and Astex Pharmaceuticals. A.G. declares honoraria from Novartis, Pfizer, Eli Lilly, PharmaMar, and Deciphera; consulting/advisory role for Novartis, Bayer, Eli Lilly, Pfizer, Nanobiotix, PharmaMar, SpringWorks Therapeutics, and Boehringer Ingelheim; institutional research funding and support for attending meetings and/or travels from PharmaMar and Nanobiotix. S.S. declares honoraria, consultancy or advisory role from Agenus, Bayer, Boehringer Ingelheim, Daiichi Sankyo, Deciphera, Gentili, GlaxoSmithKline, Ikena, PharmaMar, Pharma Essentia, Rain Therapeutics, and Servier; institutional financial interests from Advenchen, Bayer, Blueprint, Daiichi Sankyo, Deciphera, Epizyme, Eli Lilly, GlaxoSmithKline, Hutchinson MediPharma, Inhibrx, Karyopharm, Novartis, PharmaMar, Rain Therapeutics, and SpringWorks; support for attending meetings from PharmaMar. P.G.C. declares institutional research funding from Amgen/Dompé, Bayer, GlaxoSmithKline, Novartis, Pfizer, PharmaMar, Eisai, Eli Lilly, Advenchen Laboratories, Arog, Blueprint Medicines, Deciphera, Epizyme, Karyopharm Therapeutics, Daiichi Sankyo, Boehringer Ingelheim, Rain Therapeutics, Foghorn Ther Inc, Hutchinson MediPharma, Inhibrx, PTC Ther, and SpringWorks Ther. A.P.D.T. declares consulting/advisory role for Bayer, Roche, Boehringer Ingelheim. No other disclosures were reported.

Ethics Approval and Consent to Participate

The study was approved by the IRB of the Fondazione IRCCS Istituto Nazionale dei Tumori, Milan (INT #73-17) and contributing institutions. Written informed consent was obtained from all enrolled patients.

Supplementary Material

The online version contains supplementary material available at <https://doi.org/10.1016/j.modpat.2024.100647>.

References

- Stacchiotti S, Frezza AM, Blay J-Y, et al. Ultra-rare sarcomas: a consensus paper from the Connective Tissue Oncology Society community of experts on the incidence threshold and the list of entities. *Cancer*. 2021;127(16):2934–2942. <https://doi.org/10.1002/cncr.33618>
- Thway K, Jones RL, Noujaim J, Fisher C. Epithelioid sarcoma: diagnostic features and genetics. *Adv Anat Pathol*. 2016;23(1):41–49. <https://doi.org/10.1097/PAP.0000000000000102>
- Frezza AM, Botta L, Pasquali S, et al. An epidemiological insight into epithelioid sarcoma (ES): the open issue of distal-type (DES) versus proximal-type (PES). *Ann Oncol*. 2017;28:v525. <https://doi.org/10.1093/annonc/mdx387.013>
- Frezza AM, Jones RL, Lo Vullo S, et al. Anthracycline, gemcitabine, and pazopanib in epithelioid sarcoma: a multi-institutional case series. *JAMA Oncol*. 2018;4(9):e180219. <https://doi.org/10.1001/jamaoncol.2018.0219>
- Gounder M, Schöffski P, Jones RL, et al. Tazemetostat in advanced epithelioid sarcoma with loss of INI1/SMARCB1: an international, open-label, phase 2 basket study. *Lancet Oncol*. 2020;21(11):1423–1432. [https://doi.org/10.1016/S1470-2045\(20\)30451-4](https://doi.org/10.1016/S1470-2045(20)30451-4)
- Pawel BR. SMARCB1-deficient tumors of childhood: a practical guide. *Pediatr Dev Pathol*. 2018;21(1):6–28. <https://doi.org/10.1177/109326617749671>
- Blackledge NP, Klose RJ. The molecular principles of gene regulation by polycomb repressive complexes. *Nat Rev Mol Cell Biol*. 2021;22(12):815–833. <https://doi.org/10.1038/s41580-021-00398-y>
- Wilson BG, Wang X, Shen X, et al. Epigenetic antagonism between polycomb and SWI/SNF complexes during oncogenic transformation. *Cancer Cell*. 2010;18(4):316–328. <https://doi.org/10.1016/j.ccr.2010.09.006>
- Rasmussen SV, Jin JX, Bickford LR, et al. Functional genomic analysis of epithelioid sarcoma reveals distinct proximal and distal subtype biology. *Clin Transl Med*. 2022;12(7):e961. <https://doi.org/10.1002/ctm.2961>
- Modena P, Lualdi E, Facchinetto F, et al. SMARCB1/INI1 tumor suppressor gene is frequently inactivated in epithelioid sarcomas. *Cancer Res*. 2005;65(10):4012–4019. <https://doi.org/10.1158/0008-5472.CAN-04-3050>
- Del Savio E, Maestro R. Beyond SMARCB1 loss: recent insights into the pathobiology of epithelioid sarcoma. *Cells*. 2022;11(17):2626. <https://doi.org/10.3390/cells11172626>
- Grünewald TGP, Postel-Vinay S, Nakayama RT, et al. Translational aspects of epithelioid sarcoma: current consensus. *Clin Cancer Res*. 2024;30(6):1079–1092. <https://doi.org/10.1158/1078-0432.CCR-23-2174>
- Miettinen M, Fanburg-Smith JC, Virolainen M, Shmookler BM, Fetisch JF. Epithelioid sarcoma: an immunohistochemical analysis of 112 classical and variant cases and a discussion of the differential diagnosis. *Hum Pathol*. 1999;30(8):934–942. [https://doi.org/10.1016/s0046-8177\(99\)90247-2](https://doi.org/10.1016/s0046-8177(99)90247-2)
- WHO Classification of Tumours Editorial Board. WHO Classification of Tumours of Soft Tissue and Bone. 5th ed. IARC Press; 2020.**
- Dei Tos AP. Soft Tissue Sarcomas Hardback with Online Resource: A Pattern-Based Approach to Diagnosis. Cambridge University Press; 2018.**
- Frezza AM, Sbaraglia M, Lo Vullo S, et al. The natural history of epithelioid sarcoma. A retrospective multicentre case-series within the Italian Sarcoma Group. *Eur J Surg Oncol*. 2020;46(7):1320–1326. <https://doi.org/10.1016/j.ejso.2020.03.215>
- Guillou L, Wadden C, Coindre JM, Krausz T, Fletcher CD. “Proximal-type” epithelioid sarcoma, a distinctive aggressive neoplasm showing rhabdoid features. Clinicopathologic, immunohistochemical, and ultrastructural study of a series. *Am J Surg Pathol*. 1997;21(2):130–146. <https://doi.org/10.1097/0000478-199702000-00002>
- Gasparotto D, Sbaraglia M, Rossi S, et al. Tumor genotype, location, and malignant potential shape the immunogenicity of primary untreated gastrointestinal stromal tumors. *JCI Insight*. 2020;5(22):142560. <https://doi.org/10.1172/jci.insight.142560>
- Dobin A, Davis CA, Schlesinger F, et al. STAR: ultrafast universal RNA-seq aligner. *Bioinformatics*. 2013;29(1):15–21. <https://doi.org/10.1093/bioinformatics/bts635>
- Li B, Dewey CN. RSEM: accurate transcript quantification from RNA-Seq data with or without a reference genome. *BMC Bioinformatics*. 2011;12:323. <https://doi.org/10.1186/1471-2105-12-323>
- Robinson MD, McCarthy DJ, Smyth GK. edgeR: a bioconductor package for differential expression analysis of digital gene expression data. *Bioinformatics*. 2010;26(1):139–140. <https://doi.org/10.1093/bioinformatics/btp616>
- Love MI, Huber W, Anders S. Moderated estimation of fold change and dispersion for RNA-seq data with DESeq2. *Genome Biol*. 2014;15(12):550. <https://doi.org/10.1186/s13059-014-0550-8>
- Raudvere U, Kolberg L, Kuzmin I, et al. g:Profilier: a web server for functional enrichment analysis and conversions of gene lists (2019 update). *Nucleic Acids Res*. 2019;47(W1):W191–W198. <https://doi.org/10.1093/nar/gkz369>
- Subramanian A, Tamayo P, Mootha VK, et al. Gene set enrichment analysis: a knowledge-based approach for interpreting genome-wide expression profiles. *Proc Natl Acad Sci U S A*. 2005;102(43):15545–15550. <https://doi.org/10.1073/pnas.0506580102>
- Harro CM, Perez-Sanz J, Costich TL, et al. Methyltransferase inhibitors restore SATB1 protective activity against cutaneous T cell lymphoma in mice. *J Clin Invest*. 2021;131(3):135711. <https://doi.org/10.1172/JCI135711>

26. Becht E, Giraldo NA, Lacroix L, et al. Estimating the population abundance of tissue-infiltrating immune and stromal cell populations using gene expression. *Genome Biol.* 2016;17(1):218. <https://doi.org/10.1186/s13059-016-1070-5>
27. Tan TZ, Miow QH, Miki Y, et al. Epithelial-mesenchymal transition spectrum quantification and its efficacy in deciphering survival and drug responses of cancer patients. *EMBO Mol Med.* 2014;6(10):1279–1293. <https://doi.org/10.15252/emmm.201404208>
28. Kalucka J, de Rooij LPMH, Goveia J, et al. Single-cell transcriptome atlas of murine endothelial cells. *Cell.* 2020;180(4):764–779.e20. <https://doi.org/10.1016/j.cell.2020.01.015>
29. Walters R, Vasilaki E, Aman J, et al. SOX17 enhancer variants disrupt transcription factor binding and enhancer inactivity drives pulmonary hypertension. *Circulation.* 2023;147(21):1606–1621. <https://doi.org/10.1161/CIRCULATIONAHA.122.061940>
30. Drosos Y, Myers JA, Xu B, et al. NSD1 mediates antagonism between SWI/SNF and polycomb complexes and is required for transcriptional activation upon EZH2 inhibition. *Mol Cell.* 2022;82(13):2472–2489.e8. <https://doi.org/10.1016/j.molcel.2022.04.015>
31. Aryee MJ, Jaffe AE, Corradi-Bravo H, et al. Minfi: a flexible and comprehensive bioconductor package for the analysis of Infinium DNA methylation microarrays. *Bioinformatics.* 2014;30(10):1363–1369. <https://doi.org/10.1093/bioinformatics/btu049>
32. Koelsche C, Schrimpf D, Stichel D, et al. Sarcoma classification by DNA methylation profiling. *Nat Commun.* 2021;12(1):498. <https://doi.org/10.1038/s41467-020-20603-4>
33. Peters TJ, Buckley MJ, Chen Y, Smyth GK, Goodnow CC, Clark SJ. Calling differentially methylated regions from whole genome bisulphite sequencing with DMRCate. *Nucleic Acids Res.* 2021;49(19):e109. <https://doi.org/10.1093/nar/gkab637>
34. Capper D, Jones DTW, Sill M, et al. DNA methylation-based classification of central nervous system tumours. *Nature.* 2018;555(7697):469–474. <https://doi.org/10.1038/nature26000>
35. Kim JH, Megquier K, Thomas R, et al. Genomically complex human angisarcoma and canine hemangiosarcoma establish convergent angiogenic transcriptional programs driven by novel gene fusions. *Mol Cancer Res.* 2021;19(5):847–861. <https://doi.org/10.1158/1541-7786.MCR-20-0937>
36. Cancer Genome Atlas Research Network. Comprehensive and integrated genomic characterization of adult soft tissue sarcomas. *Cell.* 2017;171(4):950–965.e28. <https://doi.org/10.1016/j.cell.2017.10.014>
37. Johann PD, Erkek S, Zapatka M, et al. Atypical teratoid/rhabdoid tumors are comprised of three epigenetic subgroups with distinct enhancer landscapes. *Cancer Cell.* 2016;29(3):379–393. <https://doi.org/10.1016/j.ccr.2016.02.001>
38. R Core Team. R: a language and environment for statistical computing. R Foundation for Statistical Computing, Vienna, Austria; 2021. Accessed December 13, 2022. <https://www.R-project.org/>
39. Stine ZE, Walton ZE, Altman BJ, Hsieh AL, Dang CV. MYC, metabolism, and cancer. *Cancer Discov.* 2015;5(10):1024–1039. <https://doi.org/10.1158/2159-8290.CD-15-0507>
40. Belver L, Yang AY, Albero R, et al. GATA3-controlled nucleosome eviction drives MYC enhancer activity in T-cell development and leukemia. *Cancer Discov.* 2019;9(12):1774–1791. <https://doi.org/10.1158/2159-8290.CD-19-0471>
41. Hornick JL, Dal Cin P, Fletcher CDM. Loss of INI1 expression is characteristic of both conventional and proximal-type epithelioid sarcoma. *Am J Surg Pathol.* 2009;33(4):542–550. <https://doi.org/10.1097/PAS.0b013e3181882c54>
42. Liu NQ, Paassen I, Custers L, et al. SMARCB1 loss activates patient-specific distal oncogenic enhancers in malignant rhabdoid tumors. *Nat Commun.* 2023;14(1):7762. <https://doi.org/10.1038/s41467-023-43498-3>
43. Custers L, Khabirova E, Coorens THH, et al. Somatic mutations and single-cell transcriptomes reveal the root of malignant rhabdoid tumours. *Nat Commun.* 2021;12(1):1407. <https://doi.org/10.1038/s41467-021-21675-6>
44. Weissmiller AM, Wang J, Lorey SL, et al. Inhibition of MYC by the SMARCB1 tumor suppressor. *Nat Commun.* 2019;10(1):2014. <https://doi.org/10.1038/s41467-019-10022-5>
45. Amjadi-Moheb F, Paniri A, Akhavan-Niaki H. Insights into the links between MYC and 3D chromatin structure and epigenetics regulation: implications for cancer therapy. *Cancer Res.* 2021;81(8):1925–1936. <https://doi.org/10.1158/0008-5472.CAN-20-3613>
46. Koh CM, Iwata T, Zheng Q, Bethel C, Yegnasubramanian S, De Marzo AM. Myc enforces overexpression of EZH2 in early prostatic neoplasia via transcriptional and post-transcriptional mechanisms. *Oncotarget.* 2011;2(9):669–683. <https://doi.org/10.18632/oncotarget.327>
47. Varambally S, Dhanasekaran SM, Zhou M, et al. The polycomb group protein EZH2 is involved in progression of prostate cancer. *Nature.* 2002;419(6907):624–629. <https://doi.org/10.1038/nature01075>
48. Haraguchi T, Miyoshi H, Hiraoka K, et al. GATA3 expression is a poor prognostic factor in soft tissue sarcomas. *PLoS ONE.* 2016;11(6):e0156524. <https://doi.org/10.1371/journal.pone.0156524>
49. Cho YJ, Kim SH, Kim EK, et al. Prognostic implications of polycomb proteins ezh2, suz12, and eed1 and histone modification by H3K27me3 in sarcoma. *BMC Cancer.* 2018;18(1):158. <https://doi.org/10.1186/s12885-018-4066-6>
50. Liang X, Li L, Fan Y. Diagnostic, prognostic, and immunological roles of HELLS in pan-cancer: a bioinformatics analysis. *Front Immunol.* 2022;13:870726. <https://doi.org/10.3389/fimmu.2022.870726>
51. Zhang L, Jambusaria A, Hong Z, et al. SOX17 regulates conversion of human fibroblasts into endothelial cells and erythroblasts by dedifferentiation into CD34+ progenitor cells. *Circulation.* 2017;135(25):2505–2523. <https://doi.org/10.1161/CIRCULATIONAHA.116.025722>
52. Farber G, Dong Y, Wang Q, et al. Direct conversion of cardiac fibroblasts into endothelial-like cells using Sox17 and Erg. *Nat Commun.* 2024;15(1):4170. <https://doi.org/10.1038/s41467-024-48354-6>
53. Smith ME, Brown JI, Fisher C. Epithelioid sarcoma: presence of vascular-endothelial cadherin and lack of epithelial cadherin. *Histopathology.* 1998;33(5):425–431. <https://doi.org/10.1046/j.1365-2559.1998.00544.x>
54. Kohashi K, Yamada Y, Hotokebuchi Y, et al. ERG and SALL4 expressions in SMARCB1/INI1-deficient tumors: a useful tool for distinguishing epithelioid sarcoma from malignant rhabdoid tumor. *Hum Pathol.* 2015;46(2):225–230. <https://doi.org/10.1016/j.humpath.2014.10.010>
55. Stockman DL, Hornick JL, Deavers MT, Lev DC, Lazar AJ, Wang WL. ERG and FLI1 protein expression in epithelioid sarcoma. *Mod Pathol.* 2014;27(4):496–501. <https://doi.org/10.1038/modpathol.2013.161>
56. Miettinen M, Wang Z, Sarlomo-Rikala M, Abdullaev Z, Pack SD, Fetsch JF. ERG expression in epithelioid sarcoma: a diagnostic pitfall. *Am J Surg Pathol.* 2013;37(10):1580–1585. <https://doi.org/10.1097/PAS.0b013e31828de23a>
57. Kazansky Y, Cameron D, Mueller HS, et al. Overcoming clinical resistance to EZH2 inhibition using rational epigenetic combination therapy. *Cancer Discov.* 2024;14(6):965–981. <https://doi.org/10.1158/2159-8290.CD-23-0110>
58. Alva E, Rubens J, Chi S, et al. Recent progress and novel approaches to treating atypical teratoid rhabdoid tumor. *Neoplasia.* 2023;37:100880. <https://doi.org/10.1016/j.neo.2023.100880>
59. Alimova I, Pierce A, Danis E, et al. Inhibition of MYC attenuates tumor cell self-renewal and promotes senescence in SMARCB1-deficient group 2 atypical teratoid rhabdoid tumors to suppress tumor growth in vivo. *Int J Cancer.* 2019;144(8):1983–1995. <https://doi.org/10.1002/ijc.31873>
60. Lankes K, Hassan Z, Doffo MJ, et al. Targeting the ubiquitin-proteasome system in a pancreatic cancer subtype with hyperactive MYC. *Mol Oncol.* 2020;14(12):3048–3064. <https://doi.org/10.1002/1878-0261.12835>
61. Tran HM, Wu K-S, Sung S-Y, et al. Upregulation of protein synthesis and proteasome degradation confers sensitivity to proteasome inhibitor bortezomib in myc-atypical teratoid/rhabdoid tumors. *Cancers (Basel).* 2020;12(3):752. <https://doi.org/10.3390/cancers12030752>
62. Harney AS, Karagiannis GS, Pignatelli J, et al. The selective Tie2 inhibitor rebastinib blocks recruitment and function of Tie2Hi macrophages in breast cancer and pancreatic neuroendocrine tumors. *Mol Cancer Ther.* 2017;16(11):2486–2501. <https://doi.org/10.1158/1535-7163.MCT-17-0241>
63. Saharinen P, Eklund L, Alitalo K. Therapeutic targeting of the angiopoietin-TIE pathway. *Nat Rev Drug Discov.* 2017;16(9):635–661. <https://doi.org/10.1038/nrd.2016.278>